CT Imaging of Interstitial Lung Diseases

Marieke Hovinga, Ralf Sprengers, Hans-Ulrich Kauczor, and Cornelia Schaefer-Prokop

Abstract

Until today, computed tomography (CT) is the most important and valuable radiological modality to detect, analyze, and diagnose diffuse interstitial lung diseases (DILD), based on the unsurpassed morphological detail provided by high-resolution CT technique.

In the past decade, there has been a shift from an isolated histopathological diagnosis to a multidisciplinary acquired diagnosis consensus that is nowadays regarded to provide the highest level of diagnostic accuracy in patients with diffuse interstitial lung diseases. The 2002 ATS/ERS statement on classification of idiopathic interstitial pneumonias assigned a central role to high-resolution CT (HRCT) in the diagnostic workup of idiopathic interstitial pneumonias (ATS/ERS consensus classification 2002). The more recent 2013 ERS/ATS statement reinforced that combined clinical data (presentation, exposures, smoking status, associated diseases, lung function, and laboratory findings) and radiological findings are essential for a multidisciplinary diagnosis (Travis et al., Am J Respir Crit Care Med 188(6):733–748, 2013).

The traditional HRCT consisted of discontinuous 1 mm high-resolution axial slices. The primary focus was on visual pattern analysis demanding

M. Hovinga • R. Sprengers
Department of Radiology, Meander Medical Center, Amersfoort, The Netherlands

H.-U. Kauczor
Department of Radiology, University of Heidelberg, Heidelberg, Germany

C. Schaefer-Prokop (✉)
Department of Radiology, Meander Medical Center, Amersfoort, The Netherlands

Department of Radiology, Radboud University Nijmegen, Nijmegen, The Netherlands
e-mail: cornelia.schaeferprokop@gmail.com

U.J. Schoepf, F.G. Meinel (eds.), *Multidetector-Row CT of the Thorax*, Medical Radiology,
DOI 10.1007/978-3-319-30355-0_7

for the highest possible spatial resolution. Because of the intrinsic high structural contrast of the lung, it has been possible to substantially reduce dose without losing diagnostic information. This development has been supported by new detection and reconstruction techniques. Not only detection of subtle disease and visual comparison of disease stage but also disease classification and quantification nowadays take advantage of continuous volumetric data acquisition provided by multidetector row (MD) CT technique. The following book chapter will focus on acquisition technique with special emphasis on dose and reconstruction, advantages, and new diagnostic options of volumetric MDCT technique for interstitial lung diseases. Based on evidence from the literature, certain diseases will be covered more specifically, but it has to be noted that for the pattern analysis of the various interstitial lung diseases, the plethora of other publications and books is recommended.

1 Introduction

Until today, computed tomography (CT) is the most important and valuable radiological modality to detect, analyze, and diagnose diffuse interstitial lung diseases (DILD), based on the unsurpassed morphological detail provided by high-resolution CT technique.

In the past decade, there has been a shift from an isolated histopathological diagnosis to a multidisciplinary acquired diagnosis consensus, that is nowadays regarded to provide the highest level of diagnostic accuracy in patients with diffuse interstitial lung diseases. The 2002 ATS/ERS statement on classification of idiopathic interstitial pneumonias assigned a central role to high-resolution CT (HRCT) in the diagnostic workup of idiopathic interstitial pneumonias (ATS/ERS consensus classification 2002). The more recent 2013 ERS/ATS statement reinforced that combined clinical data (presentation, exposures, smoking status, associated diseases, lung function, and laboratory findings) *and* radiological findings are essential for a multidisciplinary diagnosis (Travis et al. 2013).

The traditional HRCT consisted of discontinuous 1 mm high-resolution axial slices. The primary focus was on visual pattern analysis demanding for the highest possible spatial resolution. Because of the intrinsic high structural contrast of the lung, it has been possible to substantially reduce dose without losing diagnostic information. This development has been supported by new detection and reconstruction techniques. Not only detection of subtle disease and visual comparison of disease stage but also disease classification and quantification nowadays take advantage of continuous volumetric data acquisition provided by multidetector row (MD) CT technique.

The following book chapter will focus on acquisition technique with special emphasis on dose and reconstruction, advantages, and new diagnostic options of volumetric MDCT technique for interstitial lung diseases. Based on evidence from the literature, certain diseases will be covered more specifically, but it has to be noted that for the pattern analysis of the various interstitial lung diseases, the plethora of other publications and books is recommended.

2 Acquisition Technique

Traditionally CT and HRCT were strongly differentiated with the latter being defined by a section thickness of <1.5 mm and the use of an edge-enhancing high-resolution reconstruction kernel. Since the advent of MDCT technique, which allows for covering the whole chest in thin section technique within one breath-hold, essentially *each* chest CT is a HRCT.

Reconstruction of 1, 3, or 5 mm thick slices determines the number of axial images to be evaluated. Besides for a given acquisition dose, a 3 mm thick slice has a better signal-to-noise ratio than a 1 mm thick slice. A 1 mm thick slice, however, offers a higher spatial resolution and thus superior morphological detail. These trade-offs therefore determine the choice of reconstruction depending on the clinical indication: analysis of an (advanced) tumor stage is mostly done with thicker slices, while analysis of diffuse interstitial lung disease or focal nodular disease requires maximum detail resolution and therefore thin slices.

Before the advent of MDCT, HRCT consisted of a thin section CT obtained with 1 mm slice thickness at 10 or even 20 mm gaps. The rationale behind such a protocol was that analysis of a diffuse parenchymal process does not require continuous coverage. Secondly, discontinuous scanning warranted the relatively high-dose use to achieve the excellent signal-to-noise, image quality, and thus detail resolution.

Several developments have contributed to the fact that over the last years, discontinuous HRCT acquisition has been increasingly replaced by volumetric data acquisition, and they will be discussed more extensively below. In short, these developments refer to:

(a) Modern MDCT scanners allow for acquisition of volumetric HRCT with high image quality at acceptable dose levels, which furthermore have been continuously decreasing over the last decades due to improved detector technology and advanced reconstruction algorithms (see also "iterative noise reconstruction").
(b) Modern scanners perform faster, allowing for a single continuous scan in deep breath-hold instead of acquiring discontinuous slices with multiple scans that require repetitive breath-hold maneuvers.
(c) Volumetric 2D and 3D display techniques such as multiplanar reconstructions (MPR), maximum and minimum intensity projections (MIP and MinIP), as well as advanced volumetric quantification techniques became only possible with continuous volumetric data acquisition.
(d) Volumetric scans allow for an easier and also more precise comparison of disease development over time in follow-up studies because slices exactly matching to each other can be compared.
(e) Volumetric scans will also capture subtle and focal disease, potentially missed when data are acquired with large gaps in between.

Nevertheless a questionnaire among members of the European Society of Thoracic Imaging carried out in 2013 revealed that a subgroup of radiologists (15 %) still uses discontinuous HRCTs for analysis of interstitial lung diseases (Prosch et al. 2013). To which extent various aspects such as the scanner technology availability, expected image quality, or unwillingness to give up the old, but familiar techniques play a role in this remains unclear.

2.1 Scan Collimation and Slice Reconstruction

There are two essential factors that constitute a "high-resolution" CT study: firstly, thin axial slices using narrow detector width (0.5–1.25 mm) and reconstruction of 1–1.5 mm thick slices (Fig. 1) and, secondly, reconstruction of the scan data with a high-spatial-frequency (sharp or high-resolution) algorithm (Muller 1991).

Whether the whole lung can be covered within one breath-hold with 1 mm collimation width depends on the speed of data acquisition. While a four-slice CT scanner still needed more than 25 s to cover a chest length of 30 cm, a 16-slice scanner provided already the technical base to cover the thorax (30 cm length) in less than 15 s when a table feed of 1.5 mm was used. A 64-slice scanner allowed for a scan time below 10 s. The most modern scanners (128-slice scanners and beyond) allow for coverage of the chest in less than 3 s while acquiring data with isotropic submillimeter resolution. Thus, speed of data acquisition within one breath-hold does not represent a limitation anymore.

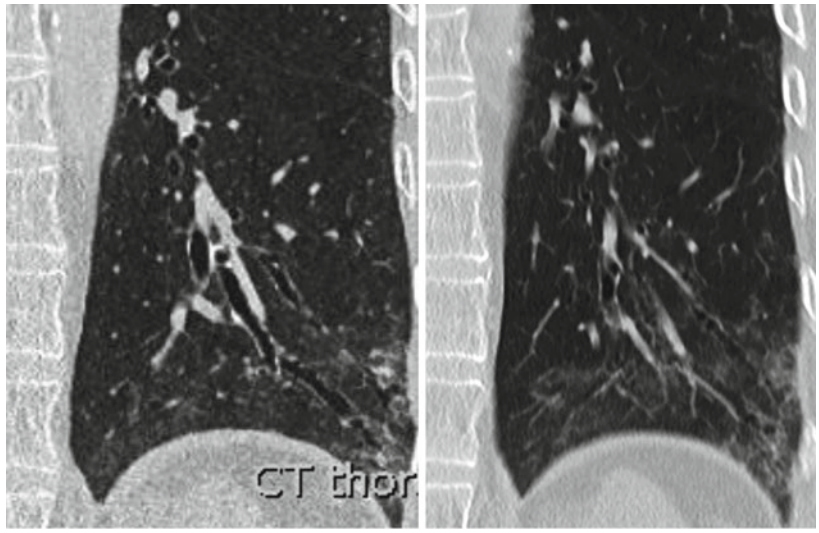

Fig. 1 Coronal reconstructions 1 mm versus 3 mm slice thickness demonstrating the impact of SL on detail resolution

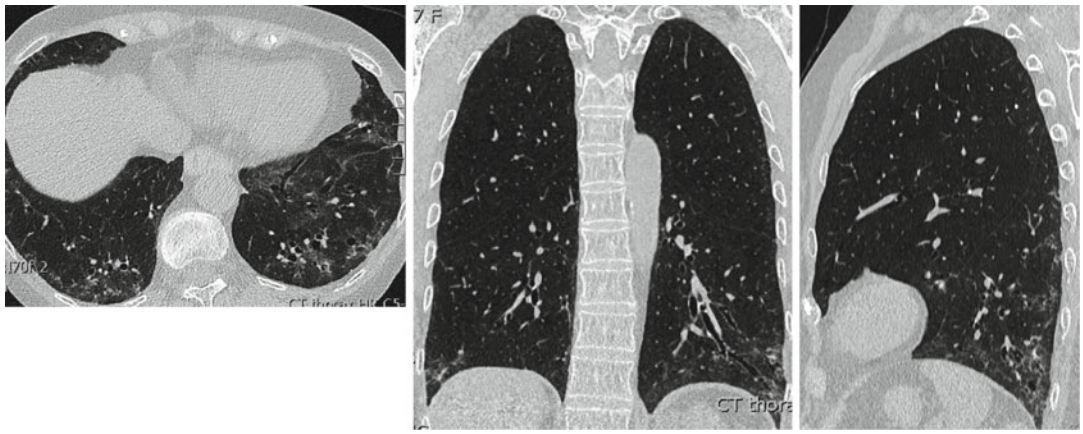

Fig. 2 Isotropic resolution in all three dimensions allows for axial, coronal, and sagittal reconstructions with equally high detail resolution. While pattern analysis is done on axial slices, the multiplanar reconstructions (MPR) nicely demonstrate the subpleural and craniocaudal distribution of disease in this patient with systemic sclerosis

The ability of HRCT to provide high morphological detail of normal and abnormal lung parenchyma is based on high-quality examinations. With optimal scan technique, the spatial resolution is as low as 0.5 mm. Due to the high contrast within the lung parenchyma, even structures as small as 0.2 mm can be visualized (Murata et al. 1989). Thus, pulmonary artery branches down to the 16th and bronchi down to the 8th generation can be depicted. Since partial volume averaging effects on the margins of such small structures are minimized, HRCT provides a very accurate image of their true size. This represents the base for CT-based quantification, e.g., of bronchial wall thickness and airway lumen in COPD patients. Since this high resolution is available isotropically, meaning in all three directions, diameters of vessels, lung nodules, or obliquely oriented bronchi are accurately reflected, irrespective of their location in or near the scan plane or even perpendicular to the scan plane (Fig. 2).

Spatial resolution is increased by the application of a high-spatial-frequency reconstruction algorithm (Mayo et al. 1987). Standard algorithms lead to smoothening of the image in respect that visible image noise is reduced and contrast resolution increased. Sharp, high-spatial-frequency, or high-resolution algorithms, on the other hand, reduce image smoothening and increase spatial resolution. Anatomic margins and tissue interfaces, such as the fissure, pleura, or septa, appear sharper. Small vessels and bronchi are seen superiorly compared to a standard algorithm.

Reducing the field of view results in smaller pixel sizes and thus increases spatial resolution. In general, the field of view should be adjusted to the size of the lungs, usually resulting in a spatial resolution of 0.5–0.3 mm. To ensure that the field of view does not cut off any parts of the lung, it is usually limited by the diameter of the external cortex of the ribs.

To further increase spatial resolution, targeting of the field of view to a single lung or particular lobes or regions can be performed. Such an approach may be used for minute evaluation of the parenchyma or peripheral bronchi beyond the regular evaluation of images demonstrating both lungs. However, with this approach, the spatial resolution will be limited by the intrinsic resolution of the detectors and whether it will gain diagnostic information will largely depend on personal preferences. There is no literature reference that generally recommends this approach, not even for certain indications. In addition, it requires additional reconstruction time, the raw data scan must be saved until targeting is performed, and it precludes the ability to compare both lungs on the same image.

2.2 Dose Aspects

One of the major arguments not to change from discontinuous HRCT (10 or 20 mm gap) to continuous volumetric data acquisition was the associated increase in dose. Since 1 mm thin sections need to have a certain signal-to-noise level to provide acceptable diagnostic image quality, it was inevitable that volumetric data acquisition would deliver a higher dose to the patient.

Table 1 Dose ranges of HRCT techniques demonstrating the potential of modern dose-reduction techniques

Effective radiation dose (mSv)	
Yearly background radiation	2.5
PA chest radiograph	0.05
Discontinuous HRCT (10 mm gap)	0.7
Volumetric HRCT	4–7
Volumetric HRCT with xyz-modulation	3–5
Volumetric HRCT with iterative noise reconstruction	1.5–3

3D dose modulation – automatically adapting the delivered dose in the transverse plane (*xy*-axis) and along patient length (*z*-axis) – is an effective means to reduce dose by about 30 % and is strongly recommended (Kubo et al. 2014) (Table 1). The abovementioned survey in 2013 confirmed that 90 % of the respondents indeed apply it. Additional options are to adapt the protocol to patient weight, patient age, or scan indication. Principally a tube voltage of 120 kV is recommended, but in young patients or patients of lower body weight, a tube voltage of 100 kV can be applied, further contributing to dose saving. The tube current is mostly set around 100 mAs. Ultimately a dose between 1.5 and 4 mSv should be aimed for (Fig. 3).

There is a multitude of publications evaluating low-dose protocols (40–60 mAs), most of them for the detection of nodules or within a screening setting. Those results cannot be directly transferred to the diagnostic workup of DILD, in which detection of ground-glass opacities and fine septal thickenings is required. Christe A et al. systematically evaluated the efficiency of a low-dose protocol for the detection of common patterns of pulmonary diseases evaluating 1 mm slices, reconstructed with filtered back projection (FBP) and a high reconstruction kernel. They concluded that a 120 kVp/40 mAs protocol was feasible for detecting solid nodules, air space consolidations, and airway and pleural diseases; however, pathologies consisting of ground-glass opacities and interstitial opacities required higher tube current or iterative noise reconstruction (Christe et al. 2013).

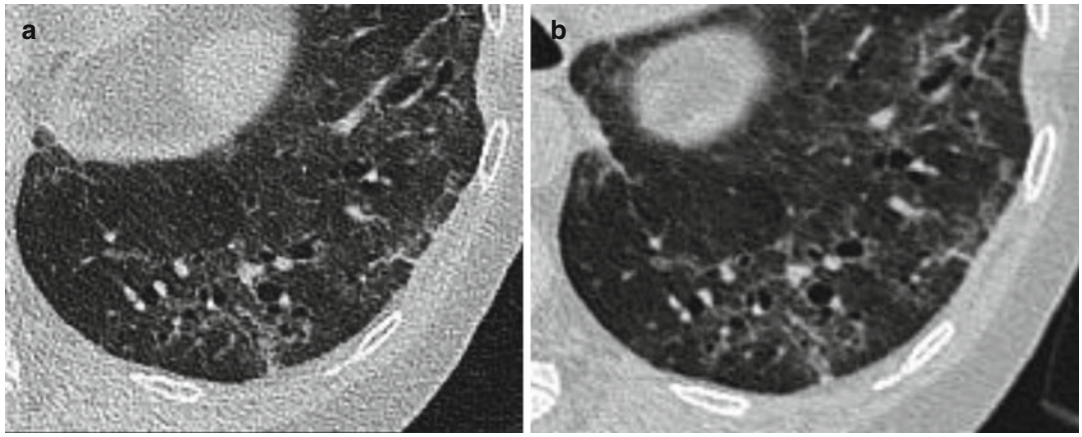

Fig. 3 Impact of dose: the right-sided image (**b**) was obtained with double acquisition dose compared to the left-sided image (**a**) (4.5 mGy versus 6.8 mGy, no iterative noise reconstruction has been applied)

New iterative reconstruction algorithms (IR) allow for greater noise reduction than standard filtered back projection (FBP) and subsequently more effective dose reduction. While increased spatial resolution is directly correlated with increase of image noise in standard filtered back projection, iterative reconstruction allows for decoupling of spatial resolution and image noise to a certain extent. Once an image has been reconstructed from measured projections, this image itself is used as "scan object" in a simulated CT measurement of the same projection, resulting in an image of calculated projections. The differences between the measured and calculated projections result in correction projections which are subsequently used to update the originally measured projections. This process is repeated until the difference between the calculated projections and measured projections is smaller than a predefined limit. With each update to the original image, image-processing algorithms enhance spatial resolution in higher contrast areas of the image and reduce noise in low contrast areas. While the first generations of IR produced images of lower noise, they were criticized for modifying the visual appearance of images, either being smoothed or pixelated especially with increased weighting of iterative noise reconstruction (Pontana et al. 2011; Prakash et al. 2010) (Fig. 4). The second generation of so-called model-based IR – active in the raw data space – aims for reducing noise and maintaining image sharpness, thus having less impact on the visual image impression.

Some studies evaluated the visualization of certain elements of lung infiltration and diffuse lung disease: an improved detection of ground-glass opacities, pulmonary nodules, and emphysema had already been reported with first-generation IR in vivo (Pontana 2011) and by experimental studies (Christe et al. 2012). Similarly an excellent inter-method agreement comparing IR and FBP images for the detection of emphysema, GGO, bronchiectasis, honeycombing, and nodules has been described (Ohno et al. 2012). No study evaluating the impact on the diagnostic evaluation of diffuse interstitial lung disease has been published yet, but nevertheless it can be anticipated that modern IR allows for substantial (around 50 %) dose reduction of volumetric HRCT for DILD, which represents an important step forward in terms of radiation protection, especially for young patients and patients with multiple follow-up studies.

2.3 Prone Position

In the normal lung with the patient supine, there is a gradual increase in attenuation and vessel size from ventral to dorsal lung regions. This attenuation gradient is caused by the effect of

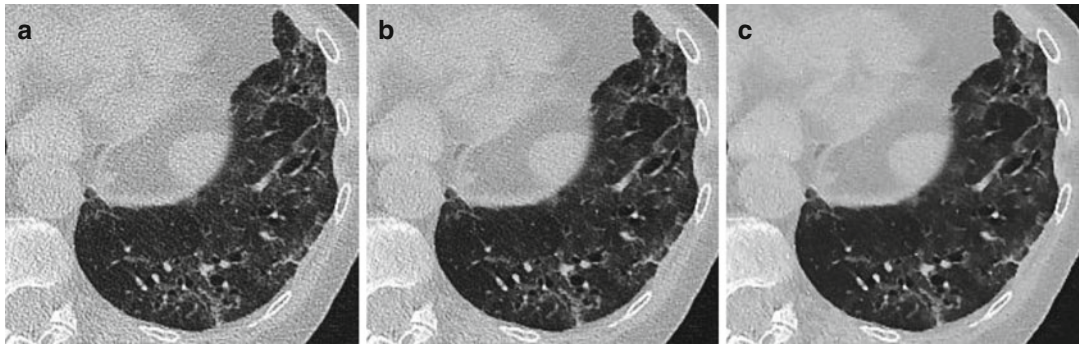

Fig. 4 Impact of iterative noise reconstruction (IR) on image noise but also on visualization of attenuation differences and detail resolution: (**a**) IR factor 1, (**b**) IR factor 3, and (**c**) IR factor 5

gravity on blood flow and gas volume as well as some non-gravity-dependent effects. This density gradient is accentuated on expiration (Verschakelen et al. 1998). Hypoventilation and atelectasis in the dependent lung can cause areas of dependent density or subpleural lines, which can mimic early lung fibrosis.

With the patient in prone position, these hydrostatic densities will immediately disappear, while abnormalities caused by real pathology will remain. Therefore, in some cases it may be necessary to obtain images in prone position to differentiate actual disease from physiologically dependent densities or atelectasis. This is especially true when the detection of ground-glass opacities or curvilinear subpleural lines are of diagnostic relevance (e.g., in patients with subtle disease or in patients with asbestosis).

Publications dating from more than 15 years ago – thus obtained with slower scanners and discontinuous HRCT technique – found that prone scanning was useful in almost 20% of patients (Volpe et al. 1997). This proportion is certainly too high, given the fast scanning technique available today. Prone scanning is not indicated routinely anymore. Some colleagues may prefer it in selected cases, e.g., patients with questionable, subtle disease exclusively in the dorsobasal area of the lung which would be decisive for the presence or absence of disease.

A questionnaire obtained in 2013 did not reveal a real consensus about the use of additional CT acquisitions in the prone position, though it was recommended to be performed on demand only (Prosch et al. 2013). This, however, requires the scans to be closely monitored or that the patient is called back for additional scanning. In patients with emphysema, airway disease, or diffuse obstructive lung disease, prone scans are usually not needed.

2.4 Expiratory Scans

Scans are routinely obtained in full inspiration with the lungs fully expanded, which optimizes the contrast between low-attenuation aerated air space and high-attenuation lung structures and various abnormalities. At the same time, full inspiration minimizes the frequency of confounding densities due to transient atelectasis.

Additional expiratory HRCT scans have proved useful in the evaluation of patients with a variety of obstructive lung diseases. Focal or diffuse air trapping may be detected and can be essential in the differentiation of large or small airway disease and emphysema (Kauczor et al. 2011).

The guidelines of the British Thoracic Society recommend the routine use of expiratory scans in patient's initial HRCT evaluation (Wells and Hirani 2008). The rationale behind this is the potential value of air trapping for the differential diagnosis that can be appreciated on an expiratory scan, even in the absence of inspiratory scan abnormalities and the fact that the functional cause of respiratory disability is not always known, especially during the initial diagnostic

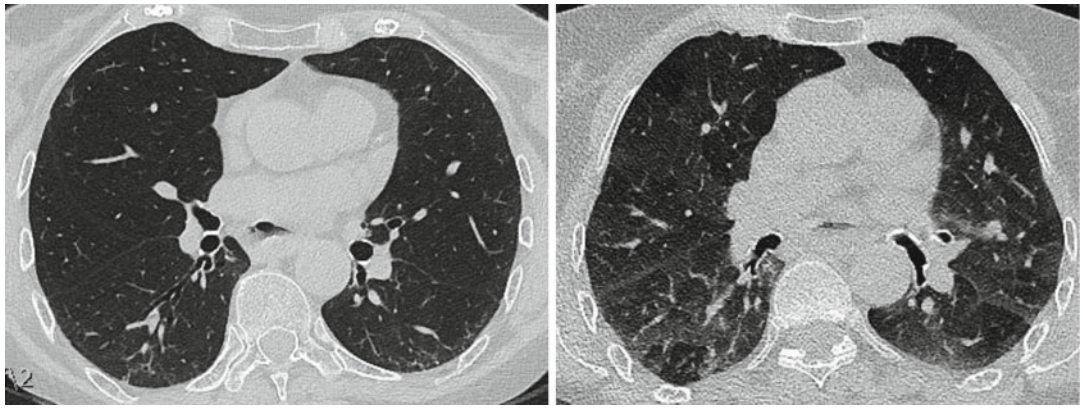

Fig. 5 Images in full inspiration and after full expiration: lobular areas of lower attenuation (*black*) demonstrate air trapping. Air trapping is more easily and sometimes exclusively seen in expiration

phase. Within the context of management of interstitial lung disease, the British Thoracic Society suggest that after a diagnosis has been set, additional expiratory CT acquisitions should only be performed to evaluate inconclusive findings on inspiratory CT.

Because of dose considerations, most investigators obtain some expiratory scans on predetermined levels or discontinuous clusters (Prosch et al. 2013). There are various ways how to plan these scans: either in areas of pathology seen in inspiration or on specific predefined levels following anatomic landmarks (e.g., carina, aortic arch) in order to facilitate reproducibility in follow-up scans. How many levels need to be covered is unclear and ranges from 2 to 5. Alternatively also the expiratory scan can be obtained with volumetric data acquisition. It has the advantage of decreasing the risk of motion artifacts frequently seen in discontinuous expiratory scans, allows for quantification on a 3D basis, and allows for more precise, level-matched follow-up. Since the only purpose of these scans is the detection, localization, and quantification of air trapping, these scans can be obtained with a drastically reduced dose. Multiple studies have shown that tube current levels as low as 40 mAs are sufficient for the diagnostic purpose intended. Bankier et al. carried out a systematic comparison of expiratory CT scans obtained with 120 kV, 80 mAs, and simulated 60, 40, and 20 mAs scans and found that – though diagnostic confidence went down with decreasing acquisition dose and interreader variability went up – diagnostic accuracy was not affected (Bankier et al. 2007). Similar results had been published also by other authors (Nishino et al. 2004).

Scans after full expiration are obtained to display lobular areas of air trapping (Fig. 5). Air trapping refers to lobular demarcated areas of hypertransparency caused by air trapped in expiration by a check valve mechanism of small airways. Consequently the involved secondary lobule will not decrease in volume and increase in attenuation during expiration compared to the surrounding uninvolved lung parenchyma. Areas of air trapping are more easily visible in expiration than in inspiration. In some patients air trapping may be seen exclusively in expiration. The finding of air trapping as indirect sign of small airway disease is an important diagnostic finding in all diseases with an obstructive or combined obstructive/restrictive lung function impairment. Diseases in which the finding of air trapping and thus expiratory CT scans represent an important part of the diagnostic workup are exogenous allergic alveolitis, collagen vascular diseases such as Sjögren's disease and rheumatoid arthritis, but also sarcoidosis and diseases with predominant airway pathology such as asthma and cystic fibrosis.

Sharply demarcated areas of air trapping need to be differentiated from ill-defined areas of varying parenchymal density in expiration. The latter

is seen frequently and has been interpreted as "inhomogeneous emptying" of the lung in expiration. Correlation of scans during inspiration and expiration illustrating the unaltered volume and density in lobuli with air trapping represents the diagnostic clue.

Expiratory CT scans are also used for interpretation of a mosaic pattern seen in inspiration. Mosaic pattern is defined as areas of varying density, sharply demarcated by interlobular septa. To differentiate whether the area of increased attenuation represents ground glass, e.g., caused by an acute alveolar or interstitial process, or that the area with hypoattenuation represents air trapping caused by bronchiolitis, expiratory CT scans are very helpful.

An increased contrast between hypo- and hyperattenuated areas in expiration demarcates air trapping as pathology and bronchiolitis as underlying disease. There are less vascular structures visible in the "black" areas of hypoattenuation due to the Euler-Liljestrand reflex, causing vascular constriction in areas of lower ventilation. Importantly there are no signs of pulmonary hypertension.

A decreased contrast between hypo- and hyperattenuated areas in expiration demarcates ground glass as pathology and an acute alveolar/interstitial process as underlying disease. There is no difference in vascular calibers in the areas of different attenuation.

Thirdly, pronounced differences in vascular diameter between the areas of different attenuation indicate true mosaic perfusion. Additional signs of pulmonary hypertension, such as dilated central pulmonary arteries and pathological arterio-bronchial ratio, may be present. The underlying disease is recurrent pulmonary emboli. Though discrimination of the different underlying diseases is also possible by analyzing the vascular diameters only, many radiologists consider the information of increased contrast differences caused by air trapping the most valuable and reassuring.

Instead of acquiring the CT scans after full expiration in suspended respiration, other authors have proposed to acquire the data during forced expiration, more specifically to perform data acquisition during the dynamic process of forced expiration. While especially end-expiratory air trapping might be seen with higher sensitivity, the risk for considerable breathing artifacts hampering image quality has to be outweighed against the potentially increased diagnostic information. Dynamic scans were firstly introduced using an electron beam CT; however, it can also be performed with any MDCT scanner with a gantry rotation time of 1 s or less. Because images can be reconstructed at any time point during the scan, the temporal resolution is even higher than with the electron beam CT. Mostly continuous imaging is performed on a single axial level for 6–8 s as the patient expires rapidly. Acquisition dose is drastically reduced (usually 40 mAs). Lucidarme et al. (2000) found a significantly higher density difference between the different areas of attenuation and a higher extent of air trapping in dynamic scans as opposed to static scans, but the number of patients for which dynamic scan acquisition changed the diagnosis has been found to be small (Gotway et al. 2000).

A detailed instruction of the patient is important to avoid motion artifacts and to assure that the scan acquisition takes part in the desired respiratory status. A visual qualitative control for the inspired or expired state is possible by analyzing the shape of the trachea: in full inspiration the trachea demonstrates a round shape, while in expiration there is bulging of the dorsal membranous part of the trachea ventrally and intraluminally to a various extent. A too strong deformation producing a considerable reduction of the tracheal area and demonstrating a moon-like (luna) shape is associated with tracheomalacia which can be a hint toward severe obstructive lung disease (O'Donnell et al. 2014).

2.5 Motion Artifacts and ECG Gating

Motion artifacts caused by non-suspended respiration are common and can severely hamper a meaningful interpretation of the images. Respiratory motion leads to blurring of normally sharp details, pseudo-ground-glass opacities, and

linear streaks or star artifacts from edges of vessels and other high-density structures.

On lung window setting, gross respiratory motion artifacts are normally easily recognizable, and while they degrade image quality, they will not cause misinterpretation because of their obviousness. Subtle motion-related unsharpness and ground-glass opacities, however, may mimic an interstitial process; doubling of vascular structures can mimic thickened interlobular septa or walls of a dilated bronchus.

A dedicated and detailed instruction of the patient how to deeply breathe in and out and especially to hold the breath before data acquisition is therefore an important step toward high image quality (Vikgren et al. 2008).

Cardiac pulsation artifacts typically affect the paracardiac regions of the left lower lobe and to a lower extent of the lingula and middle lobe. Aortic pulsation may affect lung areas adjacent to the aortic arch or the descending thoracic aorta, being the segments six and ten of the left lower lobe. In selected cases these pulsation artifacts may be misleading and can cause false positive findings. Typical artifacts are double contours of the bronchial walls mimicking bronchiectasis and hyperlucencies close to arteries mimicking emphysema. Usually they do not cause diagnostic problems if correlated to the blurred heart contour.

Options to reduce pulsation artifacts are reduced gantry rotation time, segmented reconstruction, or ECG triggering of scan acquisition. Reduced gantry rotation time and segmented reconstruction are means to increase scanning speed, but they go along with decreased dose delivery and thus increase of image noise. Prospective ECG triggering leads to a significant prolongation of measurement time, which interferes with the breath-hold capabilities of many patients. Retrospective cardiac gating would therefore be the method of choice to avoid disturbing pulsation artifacts at the expense of a markedly increased acquisition dose. In principal, techniques for coronary CT imaging can be used, without contrast administration, adaptation of the FOV to cover both lungs, and adaptation of acquisition dose. Similarly to motion-free imaging of the coronaries, motion-free imaging of the lung parenchyma would be achieved.

Nevertheless, the few studies that compared image quality with and without ECG triggering – carried out with relatively small groups of patients – found a significantly increased image quality based on artifact reduction, however, without relevant impact on diagnostic performance or confidence (Boehm et al. 2003). With the fast rotation time of most scanners used today, cardiac pulsation artifacts are significantly reduced and there appears no indication for ECG triggering for diagnostic workup of interstitial lung diseases.

3 Image Display and Processing

3.1 Windowing

There is no single correct or ideal window setting for evaluating the lung parenchyma. Window settings have to be optimized with regard to the settings of scanners and monitors. Several combinations of window level and window width may be appropriate, and individual modifications based on personal preferences play a role.

Nevertheless, it is advisable to use a chosen lung window setting consistently in all patients to optimize comparison between different patients and between sequential examinations of the same patient. It is also very important to use window settings constantly to develop a visual default and thus understanding of normal and abnormal findings. Additional window settings may be useful in specific cases, depending on what abnormality is in question.

For the assessment of a routine lung examination, window level settings ranging from −600 to −700 HU and window widths of 1000–1500 HU are recommended. Wider window width (i.e., 2000 HU) may be applied for the evaluation of overall lung attenuation and high-contrast interfaces, especially of peripheral parenchymal abnormalities along the pleural interfaces. For example, wide windows are therefore advised for the assessment of asbestosis.

Low window level settings (e.g., −800 to −900) and narrow window width (500 HU) facilitate the detection of subtle attenuation differences and are therefore suited for the detection of

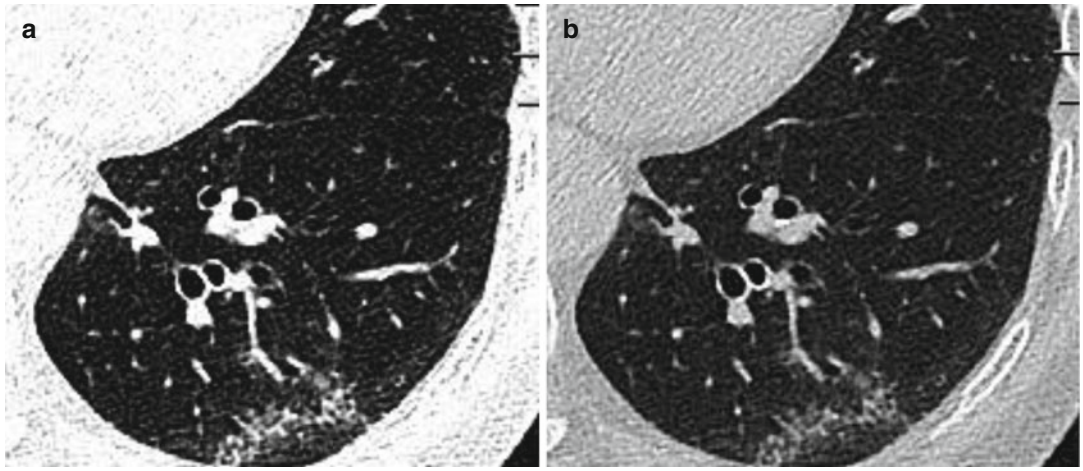

Fig. 6 Impact of window width on visualization of structures and bronchial wall thickness: (**a**) narrow window; (**b**) normal window settings

emphysema, air trapping, or air-filled cystic lesions.

The window setting has a substantial effect on the accuracy of size measurements. This is particularly important for the assessment of bronchial lumen diameter and bronchial wall thickness. It has been demonstrated that an intermediate window width between 1000 and 1400 HU together with a window level between −250 and −700 HU reflects best the true size of the bronchi and especially the thickness of the bronchial wall (Bankier et al. 1996) (Fig. 6).

As a result, it might be necessary to use different window settings for identifying pathological changes of the parenchyma or the pleura on one side and for the measurement of bronchial diameter and wall thickness on the other side. Window level settings of 40–50 HU and window width settings of 350–450 HU are generally recommended for evaluation of the mediastinum, the hili, and the pleura.

3.2 Multiplanar Reformations

Multidetector-HRCT produces an isotropic dataset that allows for contiguous visualization of the lung parenchyma in three dimensions and to create multiplanar two-dimensional (2D) reconstructions in any arbitrary plane. Mostly planar coronal and sagittal reconstructions are routinely performed and considered standard for reconstructed series of any HRCT dataset (Prosch et al. 2013; Beigelman-Aubry et al. 2005; Walsh et al. 2013) (Fig. 2).

Coronal reformations facilitate the display of disease distribution, e.g., the craniocaudal gradient representing a key finding in idiopathic pulmonary fibrosis (IPF) or the upper lobe predominance in sarcoidosis or Langerhans cell histiocytosis (LCH). Coronal MPRs are also preferred by many clinicians because they facilitate anatomic orientation (Eibel et al. 2001a) and produce images more easily comparable to chest radiographs. Advantages of sagittal MPR include the sharper delineation of the interlobar fissures and thus an improved anatomic localization of lesions close to the lobar border or for lesions with transfissural extent (Eibel et al. 2001a, b). Sagittal images also ease the evaluation of the thoracic spine and the dorsal costophrenic angle.

For the dedicated evaluation of the relationship between parenchymal lesions and airways, curved MPR can be useful following the course of the branching tubular airways (Lee and Boiselle 2010). Both coronal and sagittal MPR are superior to the axial scans alone to illustrate the location and extent of abnormalities situated in the central tracheobronchial system.

Though there is a high level of concordance between reading coronal and axial slices with regard to the identification of parenchymal disease, there is a general agreement that coronal or sagittal MPRs have a complimentary role, but are not regarded as the principle scan plane used for diagnostic evaluation.

3.3 Maximum Intensity Projection

Maximum intensity projection (MIP) is a 3D display technique, displaying the voxel of maximum intensity along the path of X-rays. To retain spatial information, MIPs are usually reconstructed with a thickness between 5 and 10 mm, dependent on the indication. Since they largely facilitate the differentiation between tubular (vascular structures) and nodular densities, their major advantage lies in demonstrating the distribution of nodules (Remy-Jardin et al. 1996; Beigelman-Aubry et al. 2005). The analysis of nodule distribution pattern in relation to the secondary lobule (e.g., perilymphatic, centrilobular, or random) is one of the key elements for the differential diagnosis; however, especially in cases with subtle findings and low numbers of nodules or on the contrary in cases with a very high number of nodules, it can be difficult to assess their distribution on axial thin slices alone, since vascular structures and nodules have the same appearance (Fig. 7).

Similarly, MIPs are very useful for the detection of (solitary) nodular densities, e.g., metastases. MIPs were found to show a large advantage especially in the central parts of the lungs; it proved to be significantly superior to regular MPR with over 25 % additional findings and increased diagnostic confidence (Peloschek et al. 2007) (Fig. 8).

In one study 103 patients with suspicion or evidence of pulmonary nodules underwent MDCT with a collimation of 1 mm. MIP and MPR were reconstructed in all three planes. The MIP were superior in the depiction of pulmonary nodules at a statistically significant level. Additional lesions were identified with MIP that were missed with transaxial slices and MPR. The improvement by MIP was based on the identification of nodules smaller than 5 mm in diameter. The improvement by MIP also led to an increase in diagnostic confidence (Eibel et al. 2001b). In a

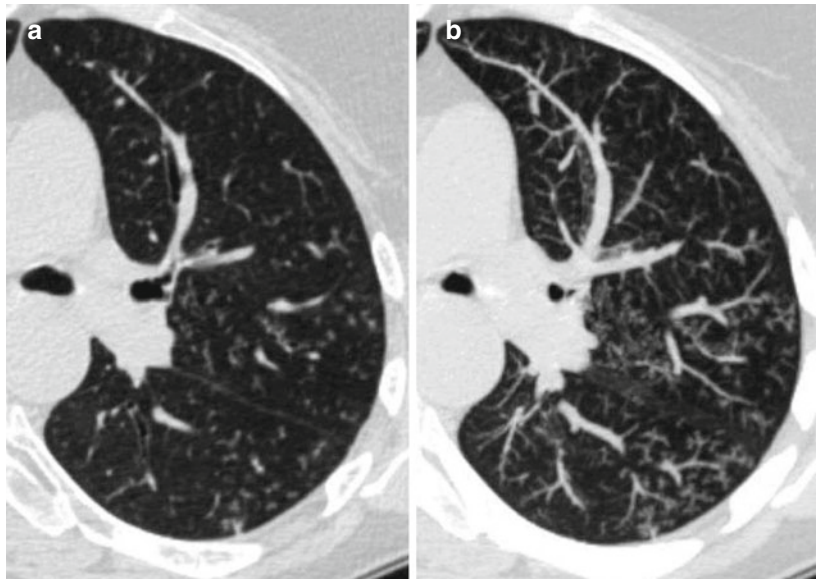

Fig. 7 1 mm axial slice (**a**) and 10 mm maximum intensity projection (MIP, **b**) demonstrating the better visualization of the distribution of a diffuse nodular pattern in MIPs in a patient with diffuse tree-in-bud due to infectious bronchiolitis nodular densities (here small granulomas) in MIPS

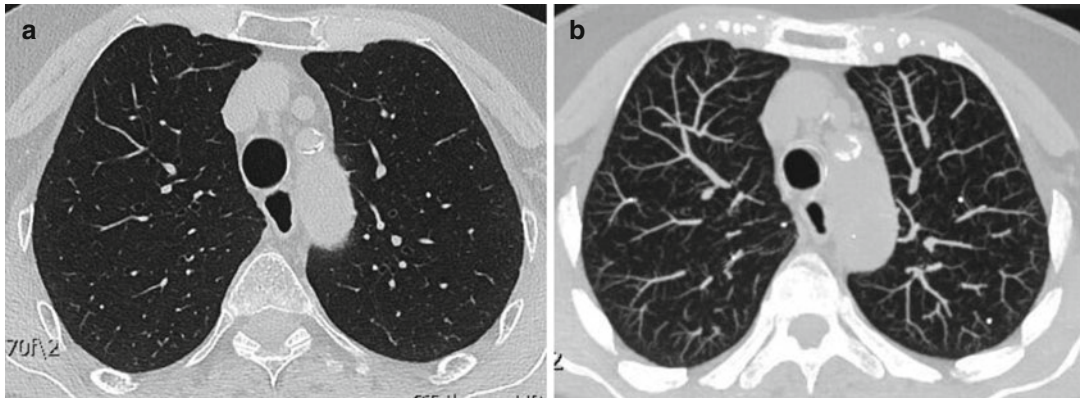

Fig. 8 1 mm axial slice (**a**) and 7 mm maximum intensity projection (MIP, **b**) demonstrating the better visualization of nodular densities (here small granulomas) in MIPs

different study, MIPs led to the detection of additional findings in 27 % of patients with nodular disease (Gavelli et al. 1998).

Finally, MIP sections of variable thickness allow assessing the size and location of pulmonary vessels. Recognizing enlarged pulmonary veins is useful in differentiating the diagnosis of pulmonary edema from other causes of diffuse ground-glass attenuation. In case of a mosaic attenuation pattern, MIP contributes to the differentiation of ground-glass attenuation (normal vascular diameter) and mosaic perfusion (altered vascular diameter). Eventually, MIP can help to differentiate between constrictive bronchiolitis and mixed emphysema (Beigelman-Aubry et al. 2005).

3.4 Minimum Intensity Projection

Minimum intensity projections (MinIPs) are less commonly used, but have been shown to facilitate the assessment of lung disease associated with decreased attenuation. MinIPs are created by projecting the voxel with the lowest attenuation value for every view throughout the volume onto a 2D image. It was demonstrated that MinIP enhances the visualization of air trapping as a result of small airway disease, yielding not only increased observer confidence but also increased interreader agreement as compared to HRCT alone (Fig. 9). MinIPs revealed additional findings in 8 % of patients with emphysema and in 25 % of cases with ground-glass opacities (Gavelli et al. 1998). These results have been confirmed by another study where MinIP improved the detection of pulmonary cysts and their differentiation from honeycombing (Vernhet et al. 1999).

There is a subtle difference in density between the endobronchial (pure) air and the lung parenchyma (HU difference 50–150). This allows visualization of the bronchi below the subsegmental level (Beigelman-Aubry et al. 2005) (Fig. 10). Recently, more attention has been paid to the options of MinIPs in facilitating the differentiation of bronchiectasis from honeycombing. The presence of honeycombing represents a key finding for the diagnosis of UIP/IPF (Raghu et al. 2011), but a relatively large interreader disagreement, even between experienced radiologists, has been described (Watadani et al. 2013).

3.5 Quantitative CT as Imaging Biomarker

CT is increasingly being used to stage and quantify the extent of DILD both in clinical practice and in treatment trials. The continuous data acquisition of CT with high isotropic resolution provides unique options for computer-supported quantification of diffuse lung disease. There has been a history in quantifying emphysema and airway disease in COPD patients with the ultimate goal to identify different phenotypes in the spectrum of

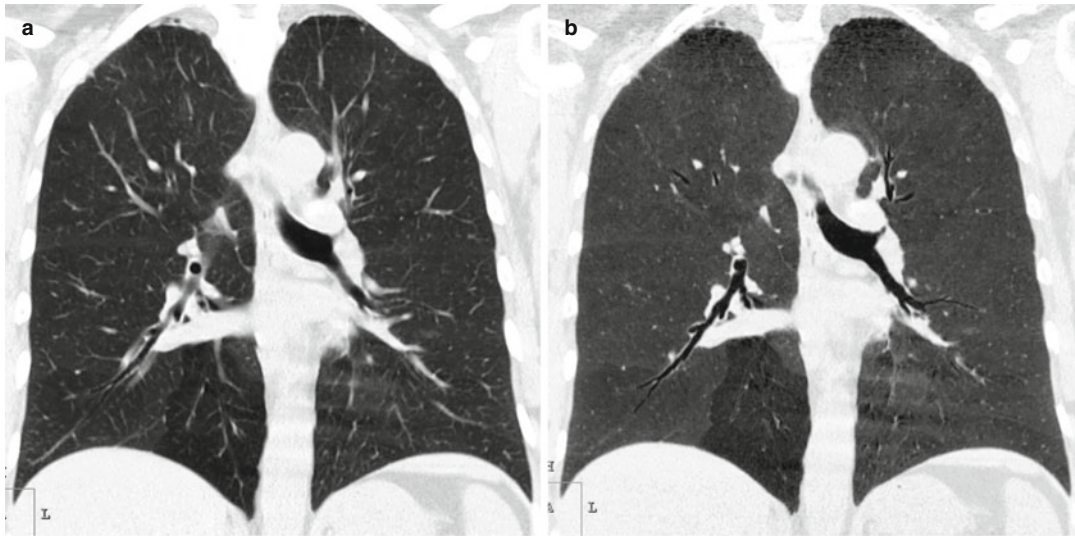

Fig. 9 3 mm coronal MPR (**a**) and 10 mm minimum intensity projection (MinIP, **b**) demonstrating the better visualization of lobular air trapping

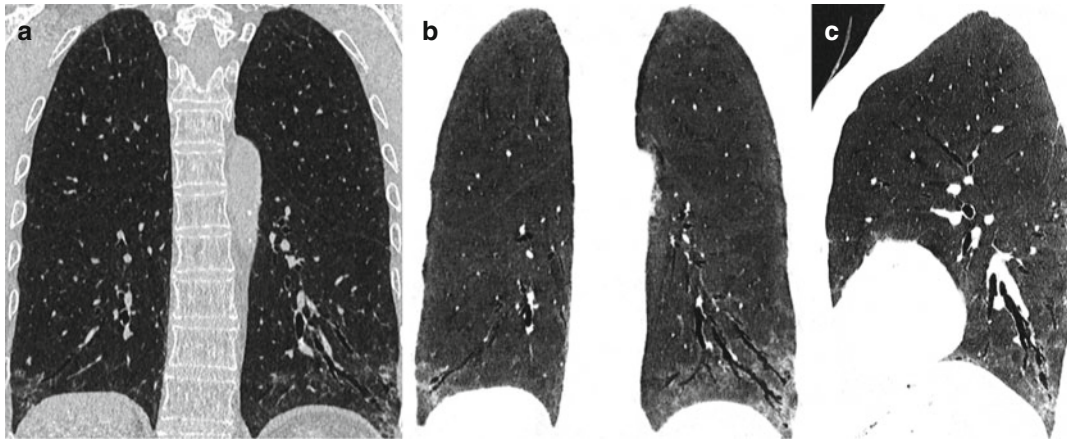

Fig. 10 1 mm coronal MPR (**a**) and 10 mm minimum intensity projection (MinIP, **b**, **c**) demonstrating the better visualization of bronchiectasis; increased peribronchial parenchymal density increases the visualization of ectatic peripheral bronchi

COPD. Recently, these efforts of computer-based analysis have been expanded to DILD.

Quantification of the extent of interstitial lung disease, both at a single time point and longitudinally, poses a challenge for several reasons:

- Mostly, DILD often consists of a mix of various patterns that show a considerable overlap between different DILD, rendering it difficult to clearly distinguish one from the other.
- The characterization of the pattern is influenced by inspiration depth, motion artifacts, and overlying other diseases such as infection.
- The extent of architectural distortions in all three spatial dimensions and within the lobular anatomy is difficult to assess.

Multiple studies have shown that type and extent of parenchymal changes, including accompanying airways pathology, correlate with lung

function, disease progression, response to therapy, and last but not least, disease prognosis. It has to be stated however that the extent of correlation is very variable for the different diseases and highly dependent on the type of pathology and thus the appreciated HRCT pattern.

Goh and colleagues proposed an interesting concept of combining a relatively simple visual quantification with pulmonary function (Goh et al. 2008). Firstly, the disease extent was differentiated into minimal or severe (less or more than 20 % involved lung area). For the subgroup of patients in which the disease extent was not readily classifiable on HRCT (so-called indeterminate), the distinction between limited and extensive was based on FVC threshold values below or beyond 70 % predicted (FVC = forced expiratory vital capacity). Using this relatively simple two-step approach, the authors were able to discriminate two groups of patients with significantly different outcomes and thus prognosis.

A similar approach of combining extent of disease on HRCT with pulmonary function tests has been successfully applied to patients with sarcoidosis and connective tissue diseases. For example, severity of traction bronchiectasis, extent of honeycombing, and DLco were found to be strongly associated with mortality in connective tissue disease related fibrotic lung disease (Walsh et al. 2014a, b). Similarly an extent of fibrosis exceeding 20 %, the diameter ratio between the aorta and main pulmonary artery, and a composite score of pulmonary function tests formed a significantly more effective prediction for mortality in sarcoidosis patients than any of the factors individually (Walsh et al. 2014a).

There has been an increasing interest for the use of automatic CT quantification as imaging biomarker to document disease response to treatment, disease progression, and eventually prognosis. Such a biomarker should be measurable but also reproducible and linked to relevant clinical outcome parameters (Goldin 2013). To meet the first two demands, rigorous standardization of imaging protocols over several sites and time points is needed, including centralized scanner and image quality checks. The underlying technique of automatic, texture analysis-based CT quantification is beyond the scope of this book chapter. There has been a number of studies evaluating the use of a computer-derived quantitative lung fibrosis score (QLF) for assessment of baseline disease extent and changes over time in patients with IPF (Kim 2015) and scleroderma patients treated with cyclophosphamide (Kim 2011). While this algorithm focuses solely on fibrotic changes, a different approach is used by the so-called CALIPER software (computer-aided lung informatics for pathology evaluation and rating), which associates a certain group of neighboring voxels to one of the basic patterns (normal, emphysema, ground glass, honeycombing, and reticular) for the complete lung volume (Bartholmai 2013). A recently published position paper by the Fleischner society (Hansell et al. 2015) acknowledges that CT has not only the potential to select the most appropriate patients to be included in treatment trials but also to represent a study end point in conjunction with other markers. This recent development has been fueled by the increasing precision with which image-processing software can quantify diffuse lung diseases.

4 Image Analysis

A widely accepted approach for analysis of HRCT in the context of DILD is based on the four patterns of pathological findings. It provides a structured and in certain ways standardized HRCT analysis and provides, together with distribution of the parenchymal changes, clinical history (acute versus chronic), and associated clinical (e.g., bronchoalveolar lavage) and imaging findings (e.g., lymphadenopathy, pleural effusion), the base for a differential diagnosis.

The four patterns differentiate between:

- Nodular opacities (I)
- Septal/reticular changes with parenchymal distortion (II)
- Diseases with increased density (III), including ground glass and consolidations
- Diseases with decreased density, mosaic pattern, and cysts (IV)

For communication with clinicians, it is important to use a cohesive terminology of signs and patterns describing the findings, so that they will know how a specific differential diagnosis has been made and what the confidence level of this diagnosis is. It has to be noted again that the final diagnosis in patients with DILD should be made within a multidisciplinary conference involving clinicians, radiologists, and pathologists and should thus be the result of a multidisciplinary approach.

A number of interstitial lung diseases are associated with such a characteristic pattern on HRCT, that diagnosis is strongly promoted by image findings, e.g., Langerhans cell histiocytosis, lymphangioleiomyomatosis, end-stage lung disease of usual interstitial pneumonia (UIP), and certain stages of sarcoidosis. Other diseases show a combination of findings that considerably overlap with a number of possible diagnoses, which is often the case in advanced disease with considerable parenchymal destruction. For example, there can be considerable overlap between sarcoidosis stage IV, UIP/IPF, and chronic exogenous allergic alveolitis.

4.1 Normal Anatomy

Localization and extent of parenchymal abnormalities are described in relation to readily appreciable anatomical structures, such as lobes and segments. The secondary lobule is the smallest anatomic unit bordered by connective tissue in the lung and represents one of the key anatomic structures in HRCT analysis that can be analyzed in its three-dimensional architecture.

In general, the secondary lobule measures between 1 and 2.5 cm in diameter, being bigger and rectangular in the periphery and smaller and more hexa- or polygonal in the central lung. The centrilobular core structures are formed by the pulmonary artery branch, the bronchiolus terminalis, lymphatics, and some connective tissue. It is important to note that under normal conditions, only the central pulmonary artery is visible on HRCT. The bronchiolus terminalis is below the spatial resolution and not visible under normal circumstances. Interlobular or perilobular septa represent the outer margin of the secondary lobule. They contain lung veins and lymphatics. In the peripheral subpleural 2 cm of lung parenchyma, only pulmonary arteries and some septal boundaries in an irregular distribution are visible. As soon as interlobular septa are regularly spaced or small airways become visible, these findings represent pathology. It is readily understandable that especially subtle pathological findings, such as an increased number of septal lines, is more easily appreciated in continuously scanned parenchyma that can be evaluated in all three projections as warranted.

4.2 Nodular Pattern

Pulmonary nodules are spherical or ovoid. They are categorized according to size, attenuation, margination, and localization. A general categorization of size results in micronodules (<3 mm), nodules (3–30 mm), and masses (>30 mm). Measurements of attenuation are problematic, but the appearance can be distinguished in being solid or of ground-glass opacity. Solid nodules may be sharply or poorly marginated, whereas ground-glass nodules are often poorly marginated. Values higher than 150 HU are typical for calcifications and indicate benign, postinflammatory granulomata. A surrounding area with increased ground-glass density is called "halo." The halo sign may be caused by acute inflammation or hemorrhage.

In general, the location or anatomic distribution of nodules is of great importance for the differential diagnosis. According to localization with regard to the anatomy of the secondary lobule, three main distribution categories of nodules are differentiated: perilymphatic, random, and centrilobular (Fig. 11). Once the predominant distribution pattern has been determined, the overall distribution within the complete lung is considered in the differential diagnosis (Fig. 12).

Perilymphatic nodules occur predominantly in relation to the lymphatic pathways within the lung, both histologically and on HRCT. They appear along the bronchovascular bundles, the

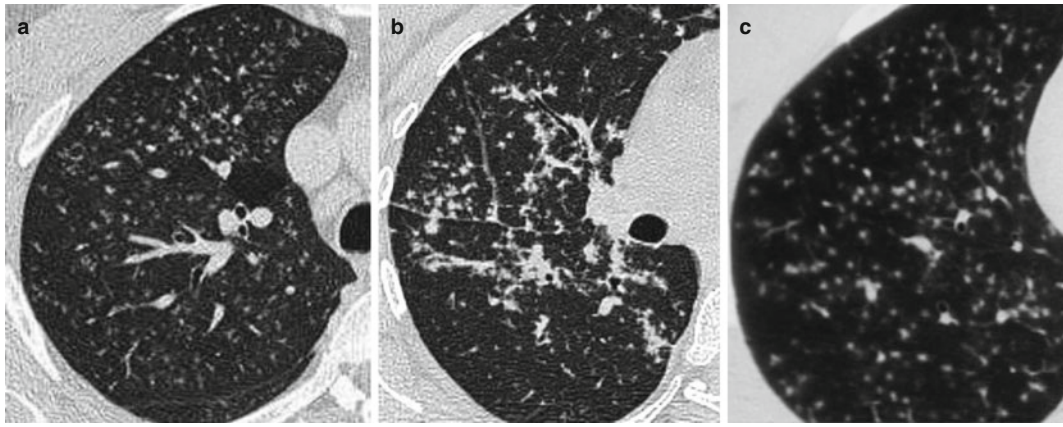

Fig. 11 Examples of a centrilobular (**a**), perilymphatic (**b**), and random (**c**) nodular distribution. (**a**) bronchiolitis, (**b**) sarcoidosis, and (**c**) miliary tuberculosis

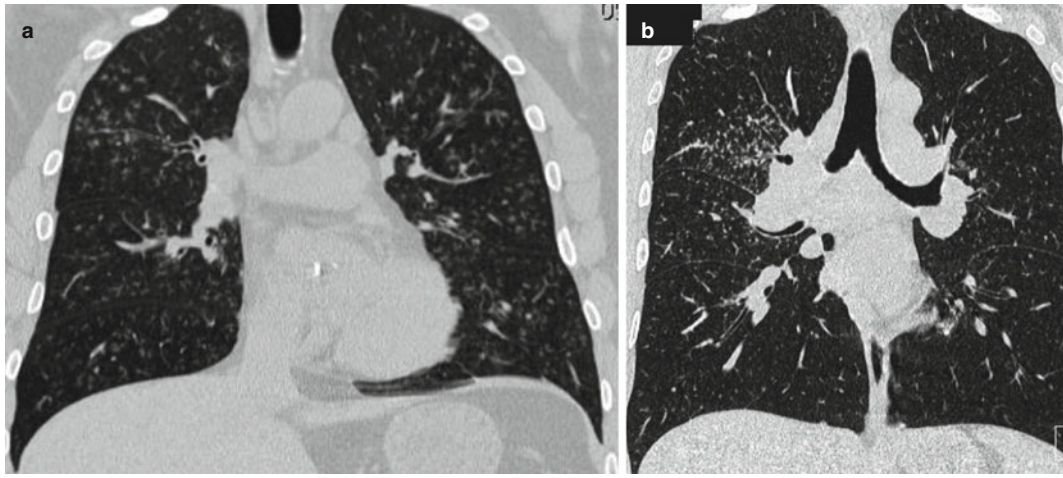

Fig. 12 1 mm coronal MPR in two patients with a nodular pattern: (**a**) shows the diffuse distribution in a patient with bronchiolitis, (**b**) shows the upper lobe predominance in a patient with sarcoidosis

interlobar fissures, the interlobular septa, and the subpleural regions. Central, perihilar nodules along the bronchovascular bundle, individually or clustered, are most typical for granuloma in sarcoidosis. The nodules usually measure less than 5 mm, are well defined, and regularly marginated. They have a predominance for the perihilar regions and the upper lobes, which is particularly well depicted on coronal reformations. Confluence of granuloma may result in larger irregularly marginated nodules, ground-glass opacities, or consolidations (Criado et al. 2010).

There might be an overlap between irregularly thickened interlobular septa caused by lymphangitis carcinomatosa and a perilobular sarcoidosis with predominantly nodules along the interlobular septa. While lymphangitis carcinomatosa is frequently associated with pleural effusion and strong thickening of the central bronchovascular interstitium, it is never characterized by lung distortion. Sarcoidosis on the other hand can show heavy distortion and usually no pleural effusion.

Typical for a *random distribution* is its uniformity throughout the lung without a preference for certain anatomical structures. The involvement

tends to be bilateral and symmetrical. A nodular pattern with a random distribution in relation to leading structures of the secondary lobule is indicative for a disease process with hematogenous spread as seen in hematogenous spread of malignant disease, miliary tuberculosis, fungal infections, cytomegaly, or herpes virus infections.

Centrilobular nodules are limited to the centrilobular regions and are never in contact with fissures or the pleura. They either originate from the respiratory bronchioles or bronchioli terminales or from the peripheral pulmonary artery branches. The nodules have a distance of at least several millimeters from interlobular septa and fissures and 5–10 mm from the pleural surface and pleura resulting in the characteristic subpleural sparing. They present as ill-defined, centrilobular ground-glass opacities in exogenous allergic alveolitis or respiratory bronchiolitis. A bit larger nodules, mostly ill-defined or consisting of solid components with a small halo around, are caused by bronchiolitis or small foci of bronchopneumonia. In silicosis, nodules can have a centrilobular as well as subpleural distribution pattern with a predominance in the posterior aspect of the upper lobes. Typically, they are smoothly marginated. The nodules range between 2 and 5 mm in diameter and can be calcified.

A *tree-in-bud* pattern– representing small-branching opacities with nodular endings – also show a centrilobular distribution; they represent small airway disease with wall thickened and/or secretion-filled small airways.

As described earlier, maximum intensity projections are most helpful in analyzing the distribution of nodules (see Sect. 3.3).

4.3 Septal/Reticular Pattern With or Without Signs of Parenchymal Distortion

Thickening of the lung interstitium caused by fluid, fibrous tissue, or cellular infiltration usually results in an increase in reticular or linear opacities on HRCT. Interlobular septal thickening is differentiated from intralobular septal thickening, although mostly seen together.

The normal interlobular septa contain venous and lymphatic structures. They measure approximately 0.1 mm in thickness and are only occasionally or partially seen on HRCT under normal conditions. Thickening of interlobular septa results in outlining the margins of the secondary lobules in part or completely; a regular network becomes apparent, and the centrilobular arteries are easily identified as small dots in the center of the secondary lobules. For differential diagnosis it is most important whether increased reticular margins are associated with signs of parenchymal distortion (e.g., traction bronchiectasis) suggesting the diagnosis of fibrosis, or whether there are no signs of distortion as, e.g., seen in crazy paving (Fig. 13).

Any diseases causing alveolar filling-in and subsequent filling of intralobular and interlobular lymphatics will cause a pattern of *crazy paving* which describes the combination of ground-glass and reticular densities. Such conditions are seen in edema, bleeding, and pneumonic infiltrations, but also in alveolar proteinosis, storage diseases, or lymphoproliferative disorders.

When caused by fibrosis, intralobular interstitial thickening results in traction bronchiectasis and bronchiolectasis, as well as displacement of fissures. This reticular pattern of thickened intra- and interlobular septa, as well as irregular thickening of the bronchovascular interstitium (interface sign) is an important diagnostic finding in the heterogeneous group of interstitial lung diseases (ILD). The most recent 2013 classification of the American Thoracic Society (ATS) and European Respiratory Society (ERS) distinguishes usual interstitial pneumonia (UIP), the specific histopathological pattern seen in idiopathic pulmonary fibrosis (IPF), from six non-IPF subtypes: acute interstitial pneumonia (AIP), respiratory bronchiolitis interstitial lung disease (RB-ILD), desquamative interstitial pneumonia (DIP), organizing pneumonia (OP), lymphoid interstitial pneumonia (LIP), and nonspecific interstitial pneumonia (NSIP) (Walsh and Hansell 2010).

Usual interstitial pneumonia (UIP) carries a particularly poor prognosis: its 5-year survival is approximately 15–30 %. Because of prognos-

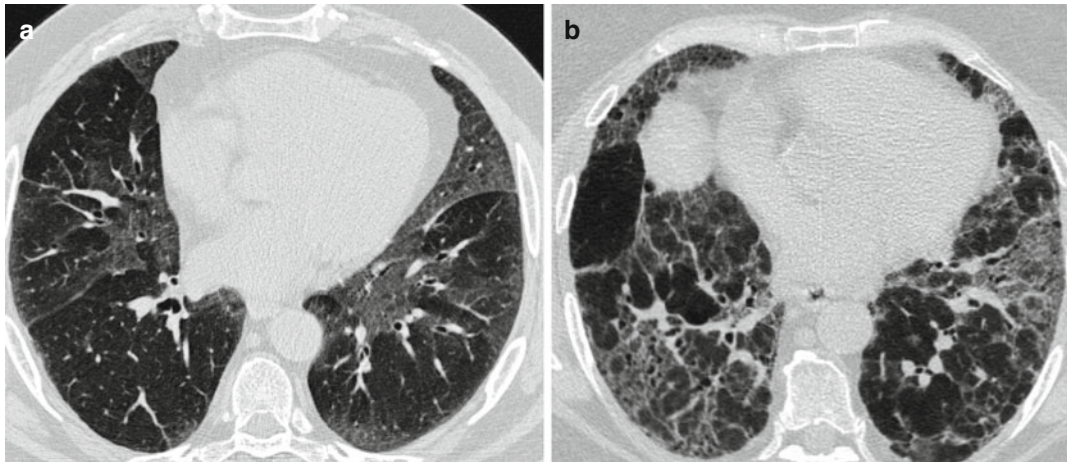

Fig. 13 1 mm axial slices in two patients with increased density in a geographic distribution: (**a**) shows no signs of distortion (desquamative interstitial pneumonia = DIP), (**b**) shows bronchiectasis and reticulation as signs of fibrosis; additionally, there are areas of air trapping (chronic exogenic allergic alveolitis)

tic and lately also therapeutic differences, UIP/IPF is separated from the remaining ILDs. The definition of IPF is a specific form of chronic, progressive fibrosing interstitial pneumonia of unknown cause that occurs primarily in older adults and is limited to the lungs and associated with the histopathologic and/or radiologic pattern of UIP. Other forms of interstitial pneumonia, including other idiopathic interstitial pneumonias and ILD associated with environmental exposure, medication, or systemic disease, must be excluded. UIP is characterized by the presence of reticular opacities associated with traction bronchiectasis. Honeycombing is critical for making a definite diagnosis following the criteria by Raghu et al. (Raghu et al. 2011) (Fig. 14). For the HRCT-based diagnosis of UIP, ground glass can be present, but is less extensive than reticulation. The distribution of UIP is characteristically predominantly basal and subpleural. Coexistent pleural abnormalities (e.g., pleural plaques, calcifications, pleural effusion) suggest an alternative etiology for the UIP pattern. Also, findings such as micronodules, air trapping, cysts, extensive ground-glass opacities, consolidation, or a peribronchovascular-predominant distribution represent findings *inconsistent* with UIP and suggest an alternative diagnosis (Fig. 15).

A UIP pattern on HRCT is highly accurate for the presence of UIP pattern on surgical lung biopsy. In the absence of honeycombing, but imaging features otherwise meeting the criteria for UIP, the HRCT findings are regarded as representing a "possible UIP," and surgical lung biopsy is necessary if a definitive diagnosis is required (Raghu et al. 2011).

Nonspecific interstitial pneumonia (NSIP) forms the second group of lung fibrosis, having a very variable clinical, radiological, and histological presentation. It may be idiopathic but is more commonly associated with collagen vascular diseases, hypersensitivity pneumonitis, drug-induced lung disease, or slowly healing DAD. The typical HRCT features are ground-glass opacities, irregular linear (reticular) opacities, and traction bronchiectasis. It has a peripheral and basal predominance, with typically (but not always present) relative sparing of the immediate subpleural space in the dorsal regions of the lower lobes. A more acute inflammatory (cellular) type of NSIP representing with predominant ground glass is differentiated from the more fibrotic type representing with reticulation and traction bronchiectasis (Fig. 16). Opposite to UIP, NSIP can also demonstrate a very patchy distribution. NSIP is typically characterized by a more uniform pattern, indicating the same stage

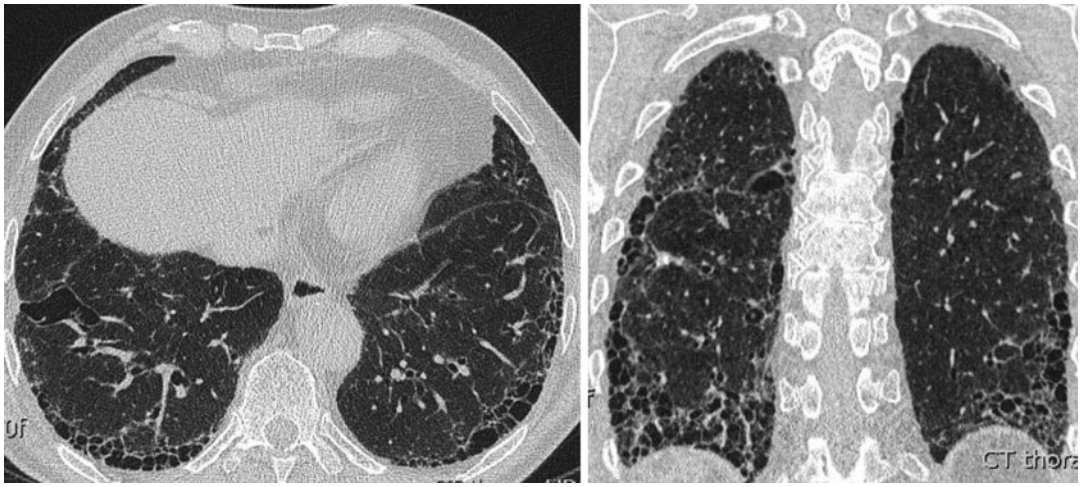

Fig. 14 Definite usual interstitial pneumonia (UIP) with honeycombing in a subpleural and mostly basal distribution. There is traction bronchiectasis and very little ground glass

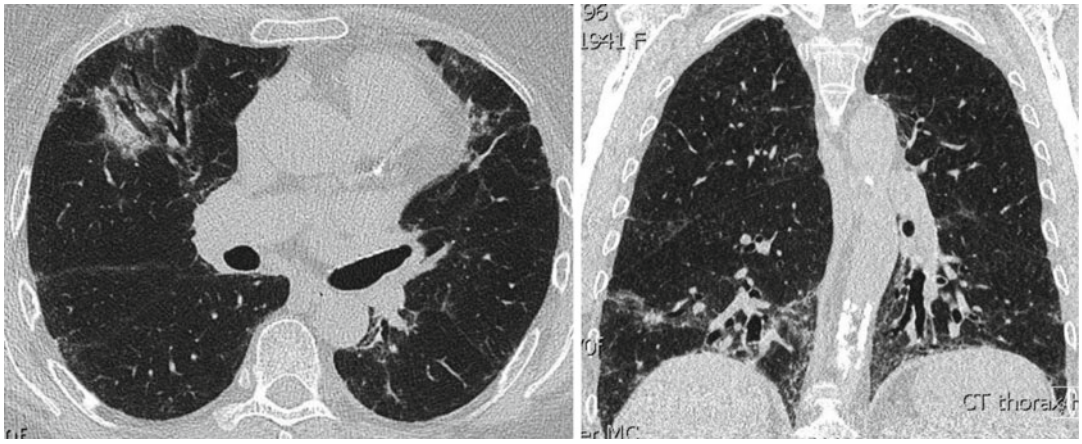

Fig. 15 Patient with fibrosis *inconsistent* with UIP through the predominant basal distribution: there is no honeycombing, but areas of ground glass and consolidations; reticulation is not predominant over ground glass

of evolution of disease, distinct from the multitemporal and morphological heterogeneity of UIP.

It has to be noted that UIP is not specific for IPF. UIP is also seen in a number of other DILD, such as asbestosis (pleural plaques and calcifications), sarcoidosis (upper lobe disease, heavy parenchymal distortion, associated nodular disease in perilymphatic distribution), or exogenic allergic alveolitis (bronchovascular-centered fibrosis, air trapping, relative sparing of the posterior costophrenic recesses).

4.4 Increased Density

Acute interstitial pneumonia (AIP) is histologically characterized by hyaline membranes within the alveoli and diffuse, active interstitial fibrosis also described as "diffuse alveolar damage" (DAD). There is clinical, pathological, and radiological overlap with ARDS, and patients often present with respiratory failure developing over days or weeks. Typical HRCT features are bilateral ground-glass opacities (patchy or diffuse) and consolidations. Focal sparing of lung lobules

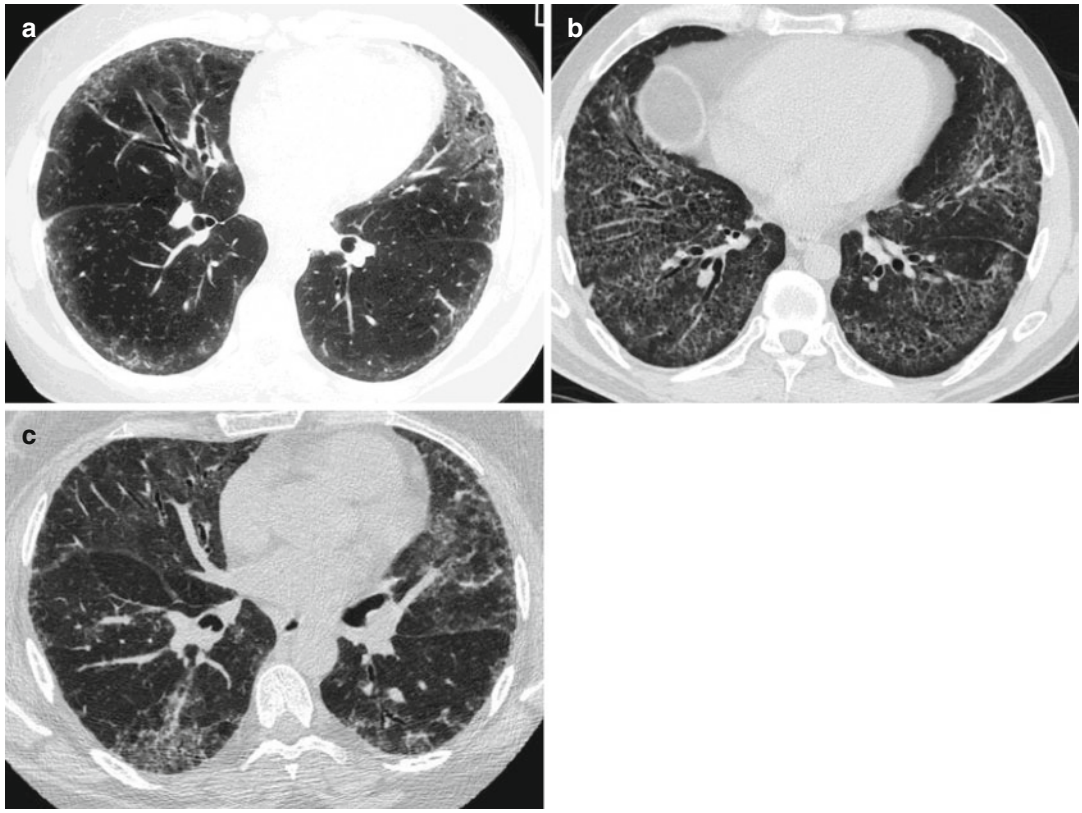

Fig. 16 The "many faces" of nonspecific interstitial pneumonia (NSIP): (**a**) subpleural bands of reticulation and ground glass (systemic sclerosis), (**b**) diffuse fine reticulation and traction bronchiectasis (systemic sclerosis), (**c**) patchy areas of ground glass and traction bronchiectasis (CREST)

frequently result in a geographic distribution. In later stages architectural distortion with traction bronchiectasis, reticulation, and even honeycombing develops.

Respiratory bronchiolitis interstitial lung disease (RB-ILD), *desquamative interstitial pneumonia (DIP)*, and, last but not least, nonspecific interstitial lung disease (NSIP) belong to the spectrum of smoking-induced lung changes. RB-ILDs consist of centrilobular acinar ground-glass nodules that may be confluent to areas of ground-glass opacities and thickening of the bronchial walls. A small percentage has a mild reticular pattern mainly in the lower lung zones. Desquamative interstitial pneumonia (DIP) is uncommon in its idiopathic form and mostly associated with smoking. HRCT features are similar to those encountered in RB-ILD, although the distribution is diffuse in DIP and more bronchiolocentric in RB-ILD. The typical HRCT feature of DIP is diffuse ground-glass opacity, sometimes in a geographic distribution; reticulation is uncommon.

Organizing pneumonia (OP) is a common reaction pattern secondary to pulmonary infection, connective tissue diseases, inflammatory bowel disease, inhalation injury, hypersensitivity pneumonitis, drug toxicity, malignancy, radiation therapy, or aspiration but can also be idiopathic. Organizing pneumonia can present with a wide variety of HRCT findings with increased density, ranging from a more nodular pattern to geographically demarcated ground-glass or focal consolidations. Suggestive for organizing pneumonia (as opposed to an infectious pneumonia) are sharply demarcated consolidations in a peripheral subpleural distribution or following the bronchovascular bundle (Fig. 17). Mostly the

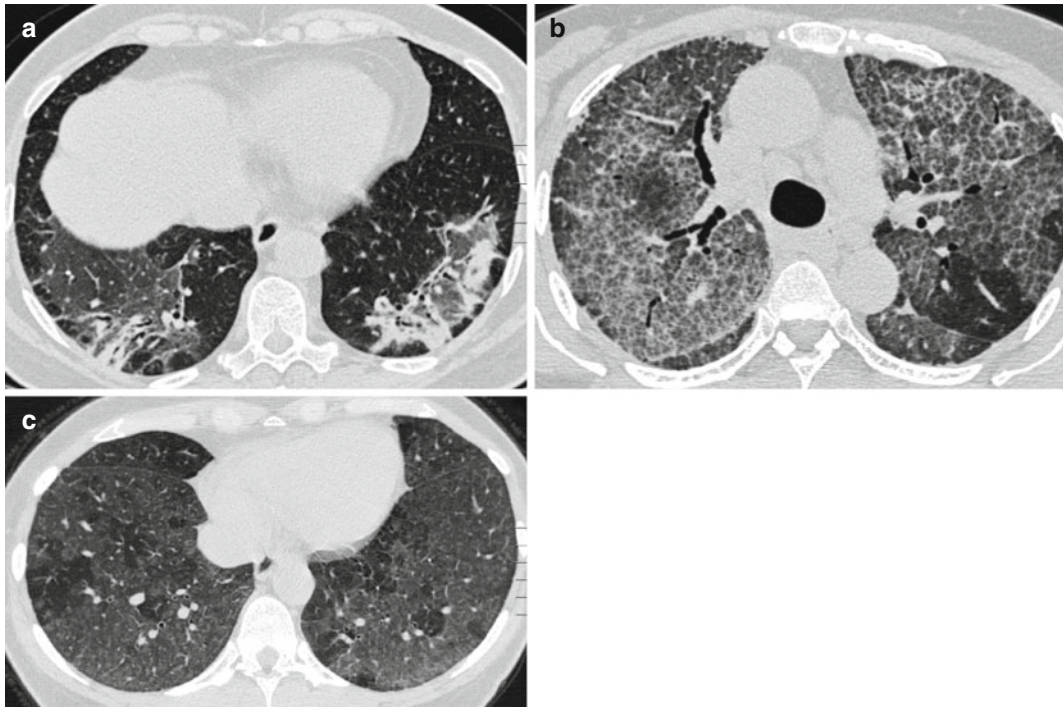

Fig. 17 Patterns with increased density: (**a**) organizing pneumonia with sharply demarcated areas of consolidations and ground glass, (**b**) crazy pacing in alveolar proteinosis, (**c**) ground glass with air trapping in subacute exogenic allergic alveolitis

areas with increased density show dilated air-filled bronchi without signs of underlying distortion. A patchy distribution is described as atoll sign, demonstrating islands with a peripheral rim-like consolidation around central areas of ground glass (reversed halo). Densities along the periphery of the secondary lobules are described as perilobular pattern.

4.5 Decreased Density/Cysts

A cystic pattern results from a heterogeneous group of diseases, all having in common the presence of focal, multifocal, or diffuse parenchymal lucencies and lung destruction. For the differential diagnosis, the presence of walls around the lucencies and the form of the lucencies (bizarre shaped or uniform round) is important.

The term "cyst" by itself is nonspecific and refers to a well-circumscribed round or irregular lesion with a visible wall. The wall is usually thin (<2–3 mm), but can have a uniform or variable thickness. Most cysts are filled with air, but can also contain liquid, semisolid, or solid material. Cysts can be very small and diffuse, but also large and confluent resulting in polygonal bizarre shapes. The presence of a definable wall demonstrated on CT differentiates cysts from emphysema.

Cysts are the leading pattern of specific lung diseases, such as Langerhans cell histiocytosis or lymphangioleiomyomatosis (LAM). Other more rare diseases with cysts are LIP and Birt-Hogg-Dube (Fig. 18).

Incidental lung cyst without other HRCT abnormalities and without a history of lung disease or signs of architectural distortion have been reported as a normal finding in elderly patients, ranging from 5 to 22 mm and located in all lobes.

In the early phase, *Langerhans cell histiocytosis (LCH)* has a typical nodular pattern with multiple, <10 mm small centrilobular nodules with irregular margins. Later these nodules increase in

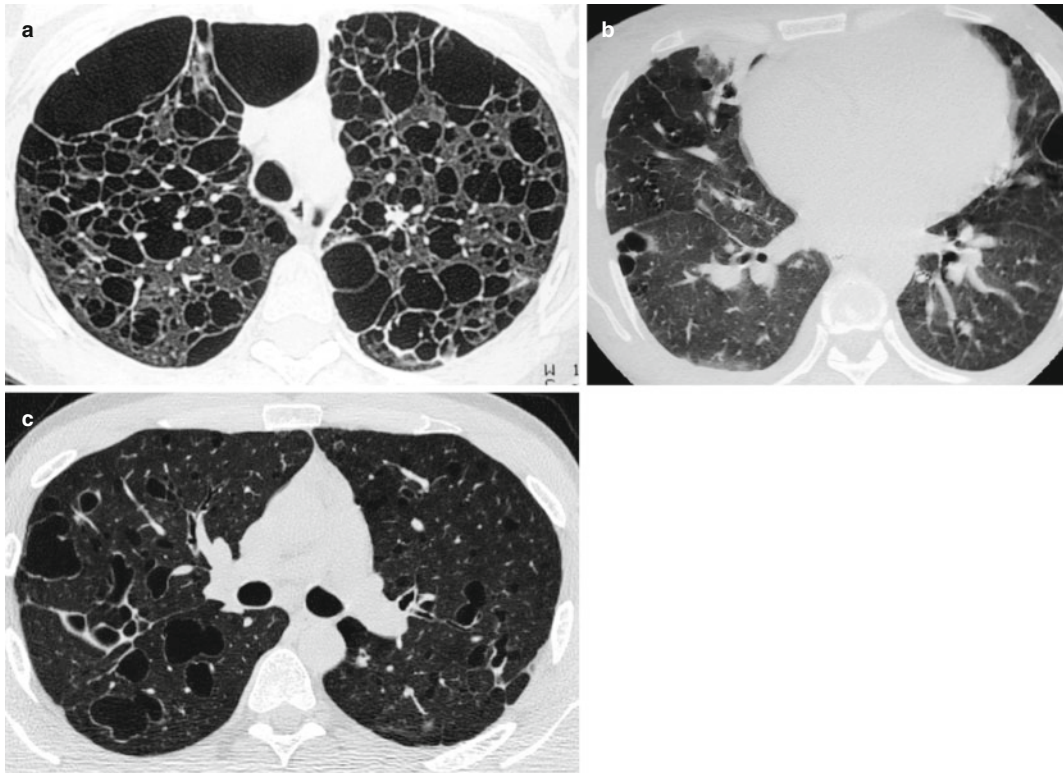

Fig. 18 Patterns with cystic parenchymal disease density: (**a**) Lymphangiomyomatosis with uniform cysts and enlarged pleural space after recurrent pneumothoraces, (**b**) diffuse ground glass and subpleural cysts in lymphocytic interstitial pneumonia (LIP), (**c**) bizarre-shaped cysts predominantly located in the upper lobes in Langerhans cell histiocytosis (LCH)

size and have a tendency to cavitate and to develop into cystic lesions with a diameter of up to 2 cm. The cysts are often confluent, have bizarre or irregular shapes, and are usually thin walled, but may be thick walled. LCH is predominantly located in the upper lobes, with sparing of the costophrenic sinus, which is better depicted on coronal reformations than on cross-sectional images. The thin walls of the cysts are prone to rupture, with an increased risk of pneumothorax. Concomitant nodules are usually irregular, measure 1–5 mm, and often have a centrilobular distribution. The interspersed pulmonary parenchyma is typically normal, without evidence of fibrosis or septal thickening.

Lymphoid interstitial pneumonia (LIP) is uncommon and considered as part of a spectrum of pulmonary lymphoproliferative disorders, ranging from benign accumulation to malignant lymphomas. Mostly it is associated with Sjögren's disease, HIV infection, or other immunological disorders. On HRCT, typical findings are sharply demarcated cysts in a subpleural distribution with intraluminal septae associated with diffuse ground glass of the lung parenchyma. Poorly defined centrilobular nodules, thickening of the bronchovascular bundles, patchy ground-glass opacities, and focal consolidations also belong to the spectrum. In cases with consolidations, a lymphoma needs to be excluded.

Lymphangioleiomyomatosis (LAM) usually occurs in young women and is frequently associated with recurrent pneumothorax and pleural effusion. The cysts are distributed bilateral diffusely throughout the lung, involving both upper and lower lobes, with also involvement of the lung bases. They are thin walled, round, and measure 0.2–5 cm. Their wall is thin, ranging from

barely visible to 4 mm in thickness. Since the thin walls of the cysts are prone to rupture, there is an increased risk of pneumothorax. Pleural effusion may also be seen. The surrounding parenchyma is typically normal. Nodules are uncommon, but may be associated with the cysts.

Sometimes it may be difficult to distinguish lymphangioleiomyomatosis and Langerhans cell histiocytosis from emphysema. A helpful finding is that the cystic spaces in LAM and LCH do not have any central nodular opacities, whereas the cystic spaces seen with centrilobular emphysema contain a small central nodular opacity representing the centrilobular artery.

Honeycomb cysts constitute the irreversible final stage of parenchymal destruction in patients with interstitial fibrosis (end-stage lung) of UIP. It is seen in IPF but also in collagen vascular diseases, asbestosis, hypersensitivity pneumonitis, or drug-related fibrosis. The cystic spaces are usually round or ovoid and measure between several millimeters and 1 cm in diameter, although more rarely they can be several centimeters in size. Within one individual, however, they are mostly uniform. They have clearly definable walls which are 1–3 mm thick. Honeycomb cysts seem to develop from alveolar disruption and massively dilated alveolar ducts and bronchioles. Honeycombing is associated with other findings of lung fibrosis, such as septal and reticular pattern, architectural distortion, and traction bronchiectasis. Most patients demonstrate several layers of irregular cystic spaces (honeycombs), which are separated from each other by irregular thick walls and intralobular septa and lines. However, note that also a singular layer of cystic spaces with thickened wall are described as honeycombing and fulfill the criteria for a definite UIP under appropriate conditions.

Though the definition of honeycombing is quite straightforward, a substantial interreader variability has been described for the diagnosis of honeycombing, which needs attention given the importance of honeycombing for the diagnosis of UIP. Even on HRCT it is not always possible to securely separate the walls of the honeycomb cysts from the thickened intralobular fibrous bands. Secondly, it is important to differentiate honeycombing from tubular bronchiectasis reaching all the way to the pleura. MinIPs have been described as helpful to differentiate between tubular bronchiectasis and focal cysts (see Sect. 3.3).

5 Summary

Continuous volumetric HRCT offers a number of advantages over discontinuous axial thin section CT slices, of which the most important ones refer to improved detection of subtle disease, better and more accurate comparability, and superior quantitative measures. A number of processing options such as MIP and MinIP ease analysis of HRCT patterns. Most recent developments of detector and reconstruction technology have made up for the disadvantage of continuous versus discontinuous data acquisition of the past, allowing for substantial dose savings. All these arguments have led to the fact that HRCT is routinely based on volumetric data acquisition. Today basically each chest CT offers the spatial resolution of a HRCT in all three dimensions, and it depends on the indication of the examination (e.g., malignancy versus diffuse parenchymal disease) whether contrast media is injected and which slice thickness and reconstruction techniques (e.g., MIP and MinIP) are applied.

References

Bankier AA, Fleischmann D, Mallek R et al (1996) Bronchial wall thickness: appropriate window settings for thin-section CT and radiologic-anatomic correlation. Radiology 199(3):831–836

Bankier AA, Schaefer-Prokop C, De Maertelaer V et al (2007) Air trapping: comparison of standard-dose and simulated low-dose thin-section CT techniques. Radiology 242(3):898–906

Bartholmai BJ, Raghunath S, Karwoski RA et al (2013) Quantitative computed tomography imaging of interstitial lung diseases. J Thorac Imaging 28(5):298–307

Beigelman-Aubry C, Hill C, Guibal A, Savatovsky J, Grenier PA (2005) Multi-detector row CT and post-processing techniques in the assessment of diffuse lung disease. Radiographics 25(6):1639–1652

Boehm T, Willmann JK, Hilfiker PR et al (2003) Thin-section CT of the lung: does electrocardiographic triggering influence diagnosis? Radiology 229(2):483–491

Christe A, Lin MC, Yen AC et al (2012) CT patterns of fungal pulmonary infections of the lung: comparison of standard-dose and simulated low-dose CT. Eur J Radiol 81(10):2860–2866

Christe A, Charimo-Torrente J, Roychoudhury K et al (2013) Accuracy of low dose computed tomography (CT) for detecting and characterizing the most common CT-Patterns of pulmonary disease. EJR 82:e142–e150

Criado E, Sánchez M, Ramírez J et al (2010) Pulmonary sarcoidosis: typical and atypical manifestations at high-resolution CT with pathologic correlation. Radiographics 30(6):1567–1586

Eibel R, Türk T, Kulinna C et al (2001a) Value of multiplanar reformations (MPR) in multi-slice spiral CT of the lung. Rofo 173(1):57–64

Eibel R, Türk TR, Kulinna C et al (2001b) Multidetector-row CT of the lungs: multiplanar reconstructions and maximum intensity projections for the detection of pulmonary nodules. Rofo 173(9):815–821

Gavelli G, Giampalma E, Cenni M et al (1998) High-resolution volumetric computerized tomography of the lung: optimization of technique and image quality as a function of its clinical-diagnostic use and dose to the patient. Radiol Med 95(4):322–328. (Italian)

Goh NS, Desai SR, Veeraraghavan S et al (2008) Interstitial lung disease in systemic sclerosis: a simple staging system. Am J Respir Crit Care Med 177(11):1248–1254

Goldin JG (2013) Computed tomography as a biomarker in clinical trials imaging. J Thorac Imaging 28(5):291–297

Gotway MB, Lee ES, Reddy GP et al (2000) Low-dose, dynamic, expiratory thin-section CT of the lungs using a spiral CT scanner. J Thorac Imaging 15(3):168–172

Hansell DM, Goldin JG, King TE Jr et al (2015) CT staging and monitoring of fibrotic interstitial lung diseases in clinical practice and treatment trials: a Position Paper from the Fleischner society. Lancet Respir Med 3(6):483–496

Kauczor HU, Wielpütz MO, Owsijewitsch M, Ley-Zaporozhan J (2011) Computed tomographic imaging of the airways in COPD and asthma. J Thorac Imaging 26(4):290–300

Kim HJ, Brown MS, Elashoff R et al (2011) Quantitative texture-based assessment of one-year changes in fibrotic reticular patterns on HRCT in scleroderma lung disease treated with oral cyclophosphamide. Eur Radiol 21(12):2455–2465

Kim SY, Diggans J, Pankratz D et al (2015) Classification of usual interstitial pneumonia in patients with interstitial lung disease: assessment of a machine learning approach using high-dimensional transcriptional data. Lancet Respir Med 3(6):473–482

Kubo T, Ohno Y, Kauczor HU, Hatabu H (2014) Radiation dose reduction in chest CT – review of available options. Eur J Radiol 83(10):1953–1961. Do

Lee KS, Boiselle PM (2010) Update on multidetector computed tomography imaging of the airways. J Thorac Imaging 25(2):112–124

Lucidarme O, Grenier PA, Cadi M et al (2000) Evaluation of air trapping at CT: comparison of continuous-versus suspended-expiration CT techniques. Radiology 216(3):768–772

Mayo JR, Webb WR, Gould R, Stein MG, Bass I, Gamsu G, Goldberg HI. (1987) High-resolution CT of the lungs: an optimal approach. Radiology 163(2):507–10

Müller NL (1991) Computed tomography in chronic interstitial lung disease. Radiol Clin North Am 29(5): 1085–93

Murata K, Khan A, Herman PG (1989) Pulmonary parenchymal disease: evaluation with high-resolution CT. Radiology 170:629–635

Nishino M, Boiselle PM, Copeland JF et al (2004) Value of volumetric data acquisition in expiratory high resolution computed tomography of the lung. J CAT 28:209–214

O'Donnell CR, Bankier AA, O'Donnell DH, Loring SH, Boiselle PM (2014) Static end-expiratory and dynamic forced expiratory tracheal collapse in COPD. Clin Radiol 69(4):357–362. doi:10.1016/j.crad.2013.11.003

Ohno Y, Takenaka D, Kanda T et al (2012) Adaptive iterative dose reduction using 3D processing for reduced- and low-dose pulmonary CT: comparison with standard-dose CT for image noise reduction and radiological findings. AJR Am J Roentgenol 199(4): W477–W485

Peloschek P, Sailer J, Weber M et al (2007) Pulmonary nodules: sensitivity of maximum intensity projection versus that of volume rendering of 3D multidetector CT data. Radiology 243(2):561–569

Pontana F, Duhamel A, Pagniez J et al (2011) Chest computed tomography using iterative reconstruction vs filtered back projection (part 2): image quality of low-dose CT examinations in 80 patients. Eur Radiol 21(3):636–643

Prakash P, Kalra MK, Ackman JB et al (2010) Diffuse lung disease: CT of the chest with adaptive statistical iterative reconstruction technique. Radiology 256(1): 261–269

Prosch H, Schaefer-Prokop CM, Eisenhuber E et al (2013) CT protocols in interstitial lung diseases – a survey among members of the European Society of Thoracic Imaging and a review of the literature. Eur Radiol 23(6):1553–1563

Raghu G, Collard HR, Egan JJ et al (2011) ATS/ERS/JRS/ALAT Committee on Idiopathic Pulmonary Fibrosis. An official ATS/ERS/JRS/ALAT statement: idiopathic pulmonary fibrosis: evidence-based guidelines for diagnosis and management. Am J Respir Crit Care Med 183(6):788–824

Remy-Jardin M, Remy J, Artaud D, Deschildre F, Duhamel A (1996) Diffuse infiltrative lung disease: clinical value of sliding-thin-slab maximum intensity projection CT scans in the detection of mild micronodular patterns. Radiology 200(2):333–339

Travis WD, Costabel U, Hansell DM, ATS/ERS Committee on idiopathic Interstitial Pneumonias et al (2013) An official American Thoracic Society/

European Respiratory Society statement: update of the international multidisciplinary classification of the idiopathic interstitial pneumonias. Am J Respir Crit Care Med 188(6):733–748

Vernhet H, Bousquet C, Vergnes C et al (1999) Contribution of high-resolution volume computed tomography (HRVCT) for the exploration of diffuse pulmonary infiltrative disorders. Rev Mal Respir 16(2):188–197. (French)

Verschakelen JA, Scheinbaum K, Bogaert J et al (1998) Expiratory CT in cigarette smokers: correlation between areas of decreased lung attenuation, pulmonary function tests and smoking history. Eur Radiol 8(8):1391–1399

Vikgren J, Johnsson AA, Flinck A et al (2008) High-resolution computed tomography with 16-row MDCT: a comparison regarding visibility and motion artifacts of dose-modulated thin slices and "step and shoot" images. Acta Radiol 49(7):755–760

Volpe J, Storto ML, Lee K, Webb WR (1997) High-resolution CT of the lung: determination of the usefulness of CT scans obtained with the patient prone based on plain radiographic findings. AJR Am J Roentgenol 169(2):369–374

Walsh SL, Hansell DM (2010) Diffuse interstitial lung disease: overlaps and uncertainties. Eur Radiol 20(8):1859–1867

Walsh SL, Nair A, Hansell DM (2013) Post-processing applications in thoracic computed tomography. Clin Radiol 68(5):433–448

Walsh SL, Wells AU, Sverzellati N et al (2014a) An integrated clinicoradiological staging system for pulmonary sarcoidosis: a case-cohort study. Lancet Respir Med 2(2):123–130

Walsh SL, Sverzellati N, Devaraj A et al (2014b) Connective tissue disease related fibrotic lung disease: high resolution computed tomographic and pulmonary function indices as prognostic determinants. Thorax 69(3):216–222

Watadani T, Sakai F, Johkoh T et al (2013) Interobserver variability in the CT assessment of honeycombing in the lungs. Radiology 266(3):936–944

Wells AU, Hirani N (2008) Interstitial lung disease guideline. Thorax 63:v1–v58